

# SOURCE LOCALIZATION ON SOLIDS UTILIZING LOGISTIC MODELING OF ENERGY TRANSITION IN VIBRATION SIGNALS

Nguyen Quang Hanh, V. G. Reju, and Andy W. H. Khong

School of Electrical and Electronic Engineering  
Nanyang Technological University, Singapore  
Email: {quanghan001, reju, andykhong}@ntu.edu.sg

## ABSTRACT

We propose a new algorithm for source localization on rigid surfaces, which allows one to convert daily objects into human-computer touch interfaces using surface-mounted vibration sensors. This is achieved via estimating the time-difference-of-arrivals (TDOA) of the signals across the sensors. In this work, we employ a smooth parametrized function to model the gradual noise-to-signal energy transition at each sensor. Specifically, the noise-to-signal transition is modeled by a four-parameter logistic function. The TDOA is then estimated as the difference in time shifts of the functions fitted to the sensor data. Experiment results show that the proposed algorithm significantly outperforms existing techniques which adopt the abrupt change model for time-of-arrival estimation.

**Index Terms**— Human-computer interface, source localization on solids, TDOA, four-parameter logistic function

## 1. INTRODUCTION

Source localization utilizing acoustic wave propagation on rigid surfaces has recently emerged as a cost-effective solution for human-computer touch interfaces (HCIs) [1–5]. In such applications, low-cost surface-mounted sensors are employed to capture vibration signals induced by impacts exerted on the surface. The signals are subsequently processed for estimating the location of the impact.

Many recent approaches achieve source localization by estimating the time-difference-of-arrival (TDOA) [6, 7]. Estimation of TDOA on rigid surfaces, however, is highly challenging as the performance of conventional techniques such as the generalized cross-correlation (GCC) [8] severely degrades due to the presence of dispersion and multipath. Dispersion refers to the dependence of wave velocity on frequency, which causes vibrations of different frequencies to arrive at a sensor at different times [9, 10]. This results in the time-of-arrival (TOA) as well as TDOA being frequency dependent. Multipath is the phenomenon where a vibration is reflected at the medium boundaries, causing distortion to the sensor-received signal [11]. While dispersion can be addressed by isolating signal components corresponding to a specific frequency [12–14], waveform distortion due to multipath causes the GCC function to have multiple false peaks, resulting in poor TDOA estimation.

Methods proposed in [15, 16] address the multipath problem by focusing on the early part of the received signal where no reflection is present to estimate its TOA. In [15], the vibration signal is assumed to be locally stationary and the Kullback-Leibler information divergence (KLID) is employed to detect the TOA which corresponds to the maximum change in frequency distribution of the received signal. The TiF-HA method [16] converts the short-time Fourier transform (STFT) coefficients of the signal into Hermitian angles (HA)

and it was noted that the standard deviation of HA across frequency bins decreases abruptly at the time instant corresponding to the TOA of the signal.

While both the KLID-based and TiF-HA methods achieve good performance for small-sized surfaces, they fail to perform as well on larger surfaces. This is due to the assumption that the noise-to-signal transition of the received signal occurs abruptly and that the TOA corresponds to the transition point. For long propagation distances such as that in large surfaces, such noise-to-signal transition, however, occurs *gradually* over a relatively longer duration. Since the number of spikes introduced by noise increases with the duration of the transition period, estimation of TOA from such spurious transition is therefore prone to error, resulting in poor TDOA estimates.

As opposed to existing algorithms, we propose to employ a smooth parametrized function to model the gradual transition of the signal at each sensor. The TDOA between a sensor pair is then estimated as the difference between the lateral shift across two respective fitted functions. While the estimated TOAs from existing techniques are severely affected by spurious spikes, the proposed fitting procedure involves received signal over the noise-to-signal transition period hence mitigating such detrimental effects. As a result, the proposed method can achieve higher accuracy in TDOA estimation resulting in better localization of the impact source for HCI applications.

## 2. THE PROPOSED STFT-LOGISTIC ALGORITHM

### 2.1. Time-frequency analysis and the logistic function

To illustrate how a parameterized function is used to model the noise-to-signal transition, we first analyze vibration signals captured using surface-mounted shock sensors on a glass plate of dimension  $1.2 \text{ m} \times 1.0 \text{ m} \times 5 \text{ mm}$ . A typical time-domain signal  $x(n)$  of length  $N$  received by one of the sensors due to a finger tap on the glass plate is shown in Fig. 1(a). The arrival of the vibration at the sensor is associated with an increase in energy of the received signal. This change in energy can clearly be observed in the time-frequency domain via computation of the STFT of the signal given by

$$\begin{aligned} \underline{x}(m) &= \mathbf{F}_K \mathbf{x}(m) \\ &= [\underline{x}(0, m), \dots, \underline{x}(K-1, m)]^T, \end{aligned} \quad (1)$$

where  $\mathbf{x}(m) = [x(m), \dots, x(m+M-1)]^T$  is a length- $M$  signal frame,  $m = 0, 1, \dots, N-M+1$  is the frame index, and  $(\cdot)^T$  denotes the transposition operator. The variable  $K$  is the number of frequency bins, and  $\mathbf{F}_K$  is the  $K \times K$  discrete Fourier transform (DFT) matrix. The spectrogram of  $x(n)$ , estimated using the magnitude of the computed STFT coefficients, is shown in Fig. 1(b) in

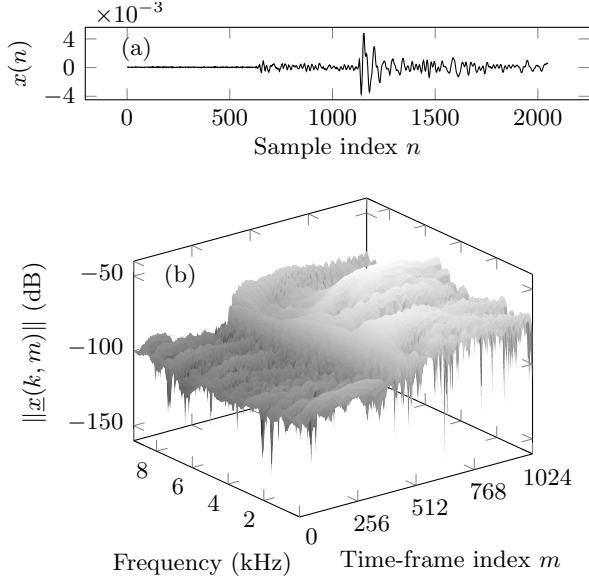


**Fig. 1:** Signal received by a sensor placed at position (1.1 m, 0.9 m) due to an impact at location (0.3 m, 0.3 m) on a glass surface of dimension 1.2 m  $\times$  1.0 m  $\times$  5 mm (a) in the time domain and (b) in the time-frequency domain.

logarithmic scale. We note from the figure that an increase in signal energy occurs as the signal arrives at the sensor. Our objective in this work is to estimate the TDOAs by analyzing such energy transition at each sensor. It is, however, worth noting that, due to velocity dispersion, energy transition varies with frequency. We therefore process the signal within a sufficiently narrow frequency band so that any dispersive effect within the band is negligible. The energy transitions across frequencies belonging to the same band can then be considered to occur at the same time.

Suppose a sufficiently narrow frequency band that has been selected covers frequency bins from  $k_b$  to  $k_e$  where  $1 \leq k_b < k_e \leq K$ . The mean spectral value across the selected frequency band at each time-frame index  $m$  is then given by

$$\chi(m) = \frac{1}{k_e - k_b + 1} \sum_{k=k_b}^{k_e} \|\underline{x}(k, m)\|. \quad (2)$$

It can be seen from Fig. 2 that  $\chi(m)$  increases from low values (corresponding to noise) to high values (corresponding to signal). Denoting the time interval corresponding to the noise-to-signal transition edge of  $\chi(m)$  as the transition period, it can be seen that the variation in energy is modest before and after the transition period. The general waveform of  $\chi(m)$  shown in Fig. 2 can then be modeled by a four-parameter logistic growth function [17, 18]

$$f(m) = A + (B - A) \left[ 1 + e^{-\gamma(m-\kappa)} \right]^{-1}, \quad (3)$$

where  $A$ ,  $B$ ,  $\gamma$ ,  $\kappa$  are the parameters that determine the shape of  $f(m)$ . The parameters

$$A = \lim_{m \rightarrow -\infty} f(m) \quad \text{and} \quad B = \lim_{m \rightarrow +\infty} f(m), \quad (4)$$

are, respectively, the minimum and maximum values of  $f(m)$ . When  $f(m)$  is fitted to the sequence  $\chi(m)$ , as shown in Fig. 2, these parameters correspond, respectively, to the noise and signal energy levels. The parameter  $\kappa$  is the translation parameter that determines the location of  $f(m)$  along the time axis such that when  $m = \kappa$ ,

$$f(\kappa) = (A + B)/2, \quad (5)$$

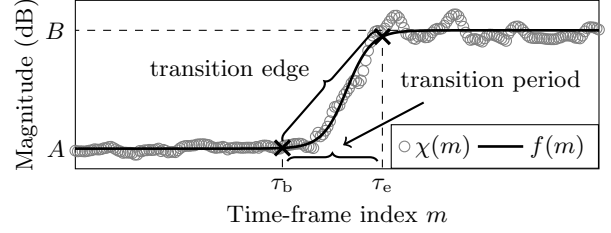


**Fig. 2:** Fitting of the logistic function  $f(m)$  to  $\chi(m)$ .

which corresponds to the midpoint of the transition edge of  $f(m)$ . The point  $m = \kappa$  therefore always lies within the transition period. The slope of  $f(m)$  at  $m = \kappa$  is given by the derivative

$$\begin{aligned} f'(\kappa) &= (B - A) \left( \gamma e^{-\gamma(m-\kappa)} \right) \left( 1 + e^{-\gamma(m-\kappa)} \right)^{-2} \Big|_{m=\kappa} \\ &= (B - A) \gamma / 4, \end{aligned} \quad (6)$$

which implies

$$\gamma = 4f'(\kappa)/(B - A). \quad (7)$$

The parameter  $\gamma$  is therefore proportional to the slope of  $f(m)$  at  $m = \kappa$  and reflects how steep the change in  $\chi(m)$  occurs when  $f(m)$  is correctly fitted. It is worth noting that abrupt transition is a special case of gradual transition where  $\gamma \rightarrow \infty$ .

Before formulating the estimation of  $A$ ,  $B$ ,  $\gamma$  and  $\kappa$  in the next section, we first describe how  $f(m)$  is deployed for TDOA estimation and why it is expected to outperform existing algorithms. Suppose that  $f_i(m)$ , with translation parameter  $\kappa_i$ , is the function fitted to  $\chi_i(m)$  of the  $i$ th sensor. The TDOA between a sensor pair  $(i, j)$  is then obtained as the difference between  $\kappa_i$  and  $\kappa_j$ . It is worth noting that, as opposed to conventional methods such as TIF-HA and KLID-based where the TDOAs are estimated via explicit estimation of TOAs, our approach utilizes the time translation of the fitting functions to estimate the TDOAs.

To understand why our proposed algorithm can achieve better localization performance, we note that existing algorithms estimate TOAs via the use of thresholding on statistics derived from the sensor output. When the transition edge is not abrupt such as the case for relatively long propagation distances in large surfaces, localization performance is highly dependent on the choice of threshold. In addition, the signal becomes more spurious due to noise over the long transition period, making the thresholding process more erroneous. Therefore, as the slope of the noise-to-signal transition edge decreases, the error in TOA estimation increases, resulting in poor TDOA estimates. On the contrary, fitting a function to the sensor data which focuses on the transition period mitigates such error. With good fitting, the time-translation error of the fitted function is averaged across all the points along the transition edge. The translation-parameter estimates are therefore robust to the slope of the transition edges. As a result, TDOAs computed via translation parameters are less error-prone compared to those obtained via threshold-based TOA estimates employed in existing techniques.

## 2.2. Four-parameter logistic model fitting

We estimate  $A$ ,  $B$ ,  $\gamma$ , and  $\kappa$  from  $\chi(m)$  by first noting that the transition period, which encapsulates the arrival of the signal, should be the focus when fitting  $f(m)$  to  $\chi(m)$ . Therefore, as opposed to [19], where a function is fitted across the entire data range, we introduce a weighting sequence  $w(m)$  so as to give higher priority to data over the transition period. The proposed algorithm involves the derivation of a cost function which is independent of  $A$  and  $B$ , followed by a non-linear optimization process for the estimation of  $\gamma$  and  $\kappa$ .

### 2.2.1. Derivation of the cost function

Let  $\varepsilon(m)$  be the residual/error, modeled as a normal random variable, while fitting  $f(m)$  to  $\chi(m)$ . With reference to (3), we obtain

$$\varepsilon(m) = \chi(m) - [A + (B - A)h(m)], \quad (8)$$

where  $h(m) = [1 + e^{-\gamma(m-\kappa)}]^{-1}$ . With  $w(m)$  properly chosen to give higher priority to data over the transition period, the weighted sum of squared fitting errors is given by

$$\begin{aligned} \mathcal{J}(A, B, \gamma, \kappa) &= \sum_{m=1}^M w(m) \varepsilon^2(m) \\ &= \tilde{\chi}^T \chi + (B - A)^2 \tilde{\mathbf{h}}^T \mathbf{h} + A^2 S_w - 2A \mathbf{w}^T \chi \\ &\quad - 2(B - A) \tilde{\mathbf{h}}^T \chi + 2A(B - A) \mathbf{w}^T \mathbf{h}, \end{aligned} \quad (9)$$

where  $\chi = [\chi(1), \dots, \chi(M)]^T$ ,  $\mathbf{w} = [w(1), \dots, w(M)]^T$ ,  $S_w = \sum_{m=1}^M w(m)$ ,  $\tilde{\chi} = [\tilde{\chi}(1), \dots, \tilde{\chi}(M)]^T$ ,  $\mathbf{h} = [h(1), \dots, h(M)]^T$ ,  $\tilde{\chi}(m) = w(m)\chi(m)$  and  $\tilde{h}(m) = w(m)h(m)$ . Differentiating (9) with respect to  $A$  and  $B$ , we obtain

$$\partial \mathcal{J} / \partial A = 2[AS_w + (A - B) \tilde{\mathbf{h}}^T \mathbf{h} + \tilde{\mathbf{h}}^T \chi - \mathbf{w}^T \chi + (B - 2A) \mathbf{w}^T \mathbf{h}] \quad (10)$$

$$\text{and} \quad \partial \mathcal{J} / \partial B = 2[(B - A) \tilde{\mathbf{h}}^T \mathbf{h} - \tilde{\mathbf{h}}^T \chi + A \mathbf{w}^T \mathbf{h}]. \quad (11)$$

Since the weighted sum  $\mathcal{J}$  is minimum when  $\partial \mathcal{J} / \partial A = 0$  and  $\partial \mathcal{J} / \partial B = 0$ , the values of  $A$  and  $B$  can be obtained from (10) and (11), respectively, as

$$A = \frac{(\mathbf{w}^T \chi)(\tilde{\mathbf{h}}^T \mathbf{h}) - (\mathbf{w}^T \mathbf{h})(\tilde{\mathbf{h}}^T \chi)}{S_w \tilde{\mathbf{h}}^T \mathbf{h} - (\mathbf{w}^T \mathbf{h})^2} \quad (12)$$

$$\text{and} \quad B = \frac{(\tilde{\mathbf{h}}^T \chi)(S_w - \mathbf{w}^T \mathbf{h}) - (\mathbf{w}^T \chi)(\mathbf{w}^T \mathbf{h} - \tilde{\mathbf{h}}^T \mathbf{h})}{S_w \tilde{\mathbf{h}}^T \mathbf{h} - (\mathbf{w}^T \mathbf{h})^2}. \quad (13)$$

Substituting (12) and (13) into (9), the cost function is now simplified to be independent of  $A$  and  $B$ , as given by

$$\begin{aligned} \mathcal{J}(\gamma, \kappa) &= \tilde{\chi}^T \chi - \frac{(\mathbf{w}^T \chi)^2 (\mathbf{h}^T \mathbf{h}) + S_w (\tilde{\mathbf{h}}^T \chi)^2}{S_w \tilde{\mathbf{h}}^T \mathbf{h} - (\mathbf{w}^T \mathbf{h})^2} \\ &\quad - \frac{2(\mathbf{w}^T \mathbf{h})(\mathbf{w}^T \chi)(\tilde{\mathbf{h}}^T \chi)}{S_w \tilde{\mathbf{h}}^T \mathbf{h} - (\mathbf{w}^T \mathbf{h})^2}. \end{aligned} \quad (14)$$

With  $\mathcal{J}(\gamma, \kappa)$  now only dependent on  $\gamma$  and  $\kappa$ , optimization methods such as that described in [20, 21] can be utilized to estimate the pair  $(\gamma, \kappa)$  that minimize the cost function in (14). To facilitate such nonlinear optimization procedure, it is important to obtain a sufficiently good initial estimate of  $(\gamma, \kappa)$ . Therefore, in the next section, we describe the process of estimating when the transition period occurs, which serves to provide an initial estimate of  $(\gamma, \kappa)$ . It is worth noting that with the transition period estimated as  $[\hat{\tau}_b, \hat{\tau}_e]$ , we can employ a weighting sequence given by

$$w(m) = \begin{cases} 1, & \hat{\tau}_b \leq m \leq \hat{\tau}_e, \\ 0, & \text{otherwise,} \end{cases} \quad (15)$$

to give higher priority to the signal data over the transition period when minimizing  $\mathcal{J}(\gamma, \kappa)$  for the purpose of fitting.

### 2.2.2. Estimating the occurrence of the transition period

Denoting the transition period by  $[\tau_b, \tau_e]$ , we now describe how to obtain its estimate  $[\hat{\tau}_b, \hat{\tau}_e]$ . Consider a frame-index  $m$  that divides  $\chi = [\chi(1), \dots, \chi(M)]^T$  into left and right partitions  $\chi_m^\ell = [\chi(1), \dots, \chi(m-1)]^T$  and  $\chi_m^r = [\chi(m+1), \dots, \chi(M)]^T$ . The

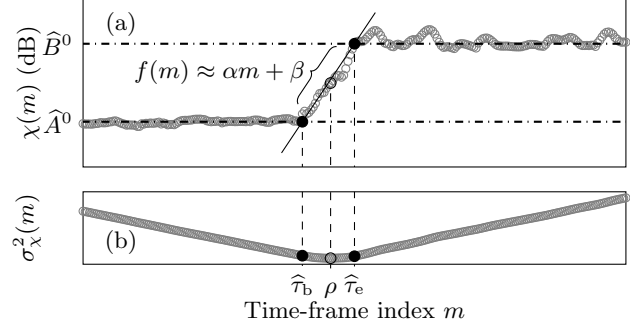


**Fig. 3:** Estimating the occurrence of transition period. The points corresponding to the end-points of the transition period are denoted by  $\bullet$ , and the point corresponding to the minimum of the total variance  $\sigma_\chi^2(m)$  is denoted by  $\circ$ .

relative position of the partition point  $m$  with respect to  $\tau_b$  and  $\tau_e$  affects the total variance of  $\chi_m^\ell$  and  $\chi_m^r$ . If  $m < \tau_b$ ,  $\chi_m^\ell$  contains only noise energy, and therefore exhibits low variance. However,  $\chi_m^r$  has high variance due to the inclusion of transition period in  $\chi(m+1), \dots, \chi(\tau_e)$ . Similarly, if  $m > \tau_e$ ,  $\chi_m^\ell$  exhibits high variance while  $\chi_m^r$  shows low variance. On the contrary, when  $m \in [\tau_b, \tau_e]$ , the number of outliers is reduced for both  $\chi_m^\ell$  and  $\chi_m^r$ , resulting in smaller variances for both the sequences. The total variance of the two partitions, given by

$$\sigma_\chi^2(m) = \text{var}\{\chi_m^\ell\} + \text{var}\{\chi_m^r\}, \quad (16)$$

can therefore reflect the position of the partitioning point with respect to the transition period, with small  $\sigma_\chi^2(m)$  corresponding to  $m \in [\tau_b, \tau_e]$ . As illustrated in Fig. 3, the point

$$\rho = \underset{m}{\text{argmin}} \sigma_\chi^2(m) \quad (17)$$

is therefore guaranteed to lie within the transition period.

Note that since  $\chi(m)$  values are highly concentrated around  $A$  (defined in (4)) for  $m \leq \tau_e$ ,  $\text{median}\{\chi_{\tau_e}^\ell\}$  is a sufficiently good estimate of  $A$ , where  $\chi_{\tau_e}^\ell = [\chi(1), \dots, \chi(\tau_e - 1)]^T$ . Exploiting the fact that the transition period is comparatively short with respect to the data length, we have  $\text{median}\{\chi_\rho^\ell\} \approx \text{median}\{\chi_{\tau_e}^\ell\}$ . An initial estimate of  $A$  can therefore be obtained as  $\hat{A}^0 = \text{median}\{\chi_\rho^\ell\}$ . Similarly,  $\hat{B}^0 = \text{median}\{\chi_\rho^r\}$ . The start of the transition period is then defined as the last time instant that  $\sigma_\chi^2(m)$  decreases below the threshold  $\hat{A}^0$ , i.e.,

$$\hat{\tau}_b = \max\{m \mid 1 \leq m < \rho; \sigma_\chi^2(m-1) < \hat{A}^0 \leq \sigma_\chi^2(m)\}. \quad (18)$$

Similarly, the end of the transition period is estimated as the first time instant that  $\sigma_\chi^2(m)$  exceeds  $\hat{B}^0$ , i.e.,

$$\hat{\tau}_e = \min\{m \mid \rho < m \leq M; \sigma_\chi^2(m) \leq \hat{B}^0 < \sigma_\chi^2(m+1)\}. \quad (19)$$

Fig. 3 illustrates the estimated  $\hat{\tau}_b$  and  $\hat{\tau}_e$  using the above process.

### 2.2.3. Estimation of $\gamma$ and $\kappa$

With the identification of the transition period, we can now adopt an approximation scheme in which the transition edge, i.e., the portion of  $f(m)$  over the period  $[\hat{\tau}_b, \hat{\tau}_e]$ , is approximated by a line that passes through the two points  $(\hat{\tau}_b, \hat{A}^0)$  and  $(\hat{\tau}_e, \hat{B}^0)$ . In other words, as can be seen from Fig. 3,

$$f(m) \approx \alpha m + \beta, \quad \forall m \in [\hat{\tau}_b, \hat{\tau}_e], \quad (20)$$

where the coefficients  $\alpha$  and  $\beta$  are given by

$$\alpha = \frac{\hat{B}^0 - \hat{A}^0}{\hat{\tau}_e - \hat{\tau}_b}, \quad \text{and} \quad \beta = \hat{A}^0 - (\hat{B}^0 - \hat{A}^0) \frac{\hat{\tau}_b}{\hat{\tau}_e - \hat{\tau}_b}. \quad (21)$$

Recall that  $\kappa \in [\tau_b, \tau_e]$ , from (5) and (20), an initial guess for  $\kappa$  is the value  $\hat{\kappa}^0 \in [\hat{\tau}_b, \hat{\tau}_e]$  that satisfies  $\alpha\hat{\kappa}^0 + \beta = (\hat{A}^0 + \hat{B}^0)/2$ , giving an initial value

$$\hat{\kappa}^0 = (\hat{\tau}_b + \hat{\tau}_e)/2. \quad (22)$$

Note that (20) also implies  $f'(m) \approx \alpha, \forall m \in [\hat{\tau}_b, \hat{\tau}_e]$ , which, together with (7) and (21), provides an initial estimate for  $\gamma$  given by

$$\hat{\gamma}^0 = 4\alpha/(\hat{B}^0 - \hat{A}^0) = 4/(\hat{\tau}_e - \hat{\tau}_b). \quad (23)$$

With the initial values  $(\hat{\gamma}^0, \hat{\kappa}^0)$ , the solution  $(\hat{\gamma}, \hat{\kappa})$  that minimizes the cost function in (14) can be obtained via iterative optimization algorithms such as the Nelder-Mead algorithm [20, 21].

### 2.3. Localization of point of impact

Consider a plate surface mounted with  $R$  sensors where the location of the  $i$ th sensor is  $(u_i, v_i)$  and an impact exerted at location  $(u_s, v_s)$ . By applying the procedure explained in the above sections for each sensor, we obtain the time-translation parameter  $\hat{\kappa}_i$  for the  $i$ th sensor. The TDOA between the  $i$ th and  $j$ th sensors is then given as

$$\hat{\tau}_{ij} = (\hat{\kappa}_i - \hat{\kappa}_j)/f_s, \quad (24)$$

where the division by the sampling frequency  $f_s$  serves the purpose of converting from sample to second.

Recall that within a sufficiently narrow selected frequency band, the signal components propagate with the same velocity, which we denote by  $c_B$ . Estimation of  $c_B$  can be achieved during calibration as described in [16] and the source location  $(u_s, v_s)$  can be estimated by minimizing the error function

$$(\hat{u}_s, \hat{v}_s) = \underset{(u, v)}{\operatorname{argmin}} \sum_{i,j} \left( [d_i(u, v) - d_j(u, v)]/c_B - \hat{\tau}_{ij} \right)^2, \quad (25)$$

where  $d_i(u, v) = \sqrt{(u - u_i)^2 + (v - v_i)^2}$  is the distance from an arbitrary location  $(u, v)$  to the  $i$ th sensor positioned at  $(u_i, v_i)$ . Such minimization can be performed, similar to that described for other HCI applications [16], using, for example, the iterative Levenberg-Marquardt optimization algorithm [22].

## 3. EXPERIMENT RESULTS

We evaluate the performance of the proposed STFT-Logistic algorithm using different sets of real data collected on two glass plates of different dimensions. The small plate is of dimension  $0.6 \text{ m} \times 0.6 \text{ m} \times 5.0 \text{ mm}$  while the large plate is of dimension  $1.2 \text{ m} \times 1.0 \text{ m} \times 5.0 \text{ mm}$ . On the surface of each of these plates, impacts are generated by either a finger or a metal stylus, making a total of four experiment setups. We employ eight surface-mounted Murata PKS1-4A10 piezoelectric shock sensors to capture impact-induced vibrations where the sensor outputs are digitized using  $f_s = 96 \text{ kHz}$ . The sensors are mounted at the corners and the midpoints of the edges,  $0.1 \text{ m}$  away from the plate boundaries. For the small plate, impacts are generated at locations  $(0.2, 0.2)$ ,  $(0.2, 0.3)$ ,  $(0.2, 0.4)$ ,  $(0.3, 0.2)$ ,  $(0.3, 0.3)$ ,  $(0.3, 0.4)$ ,  $(0.4, 0.2)$ ,  $(0.4, 0.3)$ , and  $(0.4, 0.4)$ . For the large plate, the impact locations are  $(0.3, 0.3)$ ,  $(0.3, 0.5)$ ,  $(0.3, 0.7)$ ,  $(0.5, 0.3)$ ,  $(0.6, 0.5)$ ,

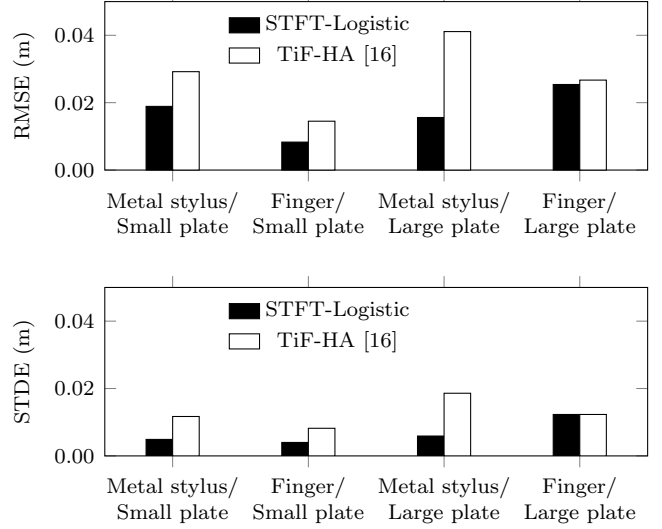


**Fig. 4:** Performance comparison of the proposed algorithm with that of TiF-HA [16] using (a) RMSE and (b) standard deviation of the localization errors (STDE).

$(0.6, 0.7)$ ,  $(0.9, 0.3)$ ,  $(0.9, 0.5)$ , and  $(0.9, 0.7)$  (all the dimensions are in meters). At each location, a set of five impacts are generated, and hence a total of forty-five test cases are performed for each experiment setup. In order to quantify the overall performance of each algorithm on a set of data, the root-mean-square error (RMSE) and the standard deviation (STDE) of the localization errors for all impacts in the set are employed.

Since the TiF-HA outperforms the KLID-based method, we only compare the performance of our proposed algorithm with that of TiF-HA [16]. It can be seen from Fig. 4 that the proposed STFT-Logistic outperforms the TiF-HA significantly albeit a modest improvement in performance for the finger tap on the large plate. These results illustrate the advantage of the adoption of gradual-change model over abrupt-change model. The modest improvement in localization performance of the proposed STFT-Logistic for finger taps on large surface may be explained as follows. Unlike a metal stylus which is rigid, a finger is soft and generates multiple vibrations due to flesh, nail and bone. These vibrations are of different types and propagate with different velocities. Over the small surface, due to the short propagation distance, the difference in arrival times at the sensor of these vibrations are negligibly small. On the contrary, for a large surface, their separation in arrival times affects the energy transition of the sensor output. This energy transition now corresponds to multiple vibrations while the transition modeling was intended for the arrival of a single vibration. Such model mismatch causes the performance of STFT-Logistic to degrade in this case and only to outperform that of TiF-HA modestly.

## 4. CONCLUSION

Our proposed TDOA-based algorithm for HCI applications employs the four-parameter logistic function to model the gradual energy transition of the sensor-received signals. The TDOA information is then estimated as the time-translational difference between the functions fitted to the sensor data. The proposed STFT-Logistic avoids the direct estimation of TOA, which is prone to error when the transition is gradual, and therefore outperforms existing techniques which adopt the abrupt change model for TOA estimation.

## 5. REFERENCES

- [1] D. T. Pham, M. Al-Kutubi, Z. Ji, M. Yang, Z. B. Wang, and S. Catheline, "Tangible acoustic interface approaches," in *Proc. Int. Virtual Conf. IPROMs*, 2005.
- [2] X. Yap, A. W. H. Khong, and W. S. Gan, "Localization of acoustic source on solids: A linear predictive coding based algorithm for location template matching," in *Proc. IEEE Int. Conf. Acoustics, Speech, and Signal Processing (ICASSP)*, 2010, pp. 2490–2493.
- [3] K. Poletkin, X. Yap, and A. W. H. Khong, "A touch interface exploiting the use of vibration theories and infinite impulse response filter modeling based localization algorithm," in *Proc. IEEE Int. Conf. Multimedia and Expo (ICME)*, 2010, pp. 286–291.
- [4] K. R. Arun, X. Yap, and A. W. H. Khong, "A touch interface exploiting time-frequency classification using Zak transform for source localization on solids," *IEEE Trans. Multimed.*, vol. 13, pp. 487–497, 2011.
- [5] K. R. Arun, V. G. Reju, and A. W. H. Khong, "Source localization on solids utilizing time-frequency analysis of parameterized warped signals," in *Proc. IEEE Int. Conf. Acoustics, Speech and Signal Processing (ICASSP)*, May 2014, pp. 689–693.
- [6] S. M. Ziola and M. R. Gorman, "Source location in thin plates using cross-correlation," *J. Acoust. Soc. Amer.*, vol. 90, pp. 2551–2556, 1991.
- [7] W. Rolshofen, D. T. Pham, M. Yang, Z. B. Wang, Z. Ji, and M. Al-Kutubi, "New approaches in computer-human interaction with tangible acoustic interfaces," in *Proc. Int. Virtual Conf. IPROMs*, 2005.
- [8] C. Knapp and G. C. Carter, "The generalized correlation method for estimation of time delay," *IEEE Trans. Acoust., Speech, Signal Process.*, vol. 24, no. 4, pp. 320–327, 1976.
- [9] Y. T. Chan, T. K. C. Lo, and H. C. So, "Passive range-difference estimation in a dispersive medium," *IEEE Trans. Signal Process.*, vol. 58, pp. 1433–1439, 2010.
- [10] Y. Jiang and A. Papandreou-Suppappola, "Discrete Time-Frequency Characterizations of Dispersive Linear Time-Varying Systems," *IEEE Trans. Signal Process.*, vol. 55, pp. 2066–2076, May 2007.
- [11] F. Foroozan and A. Asif, "Time reversal based active array source localization," *IEEE Trans. Signal Process.*, vol. 59, pp. 2655–2668, June 2011.
- [12] H. Jeong and Y. Jang, "Fracture source location in thin plates using the wavelet transform of dispersive waves," *IEEE Trans. Ultrason. Ferroelectr., Freq. Control*, vol. 47, no. 3, pp. 612–619, 2000.
- [13] Q. Wang and F. Chu, "Experimental determination of the rubbing location by means of acoustic emission and wavelet transform," *J. Sound Vibration*, vol. 248, no. 1, pp. 91 – 103, 2001.
- [14] T. Kosel, I. Grabec, and F. Kosel, "Intelligent location of simultaneously active acoustic emission sources: Part I," *Aircr. Eng. Aerosp. Technol.*, vol. 75, pp. 11 – 17, 2003.
- [15] K. R. Arun, E. Ong, and A. W. H. Khong, "Source localization on solids using Kullback-Leibler discrimination information," in *Proc. Int. Conf. Information, Communications and Signal Processing (ICICS)*, 2011, pp. 1–5.
- [16] V. G. Reju, A. W. H. Khong, and A. B. Sulaiman, "Localization of taps on solid surfaces for human-computer touch interfaces," *IEEE Trans. Multimed.*, vol. 15, pp. 1365–1376, Oct. 2013.
- [17] J. C. Bezdek, R. A. Chandrasekhar, and Y. Attikouzel, "A geometric approach to edge detection," *IEEE Trans. Fuzzy Syst.*, vol. 6, pp. 52–75, Feb 1998.
- [18] G. Dinse, "An EM algorithm for fitting a four-parameter logistic model to binary dose-response data," *J. Agric. Biol. Environ. Stat.*, vol. 16, no. 2, pp. 221–232, 2011.
- [19] F. Cavallini, "Fitting a logistic curve to data," *College Math. J.*, vol. 24, no. 3, pp. 247–253, 1993.
- [20] J. A. Nelder and R. Mead, "A simplex method for function minimization," *Comput. J.*, vol. 7, no. 4, pp. 308–313, 1965.
- [21] J. C. Lagarias, J. A. Reeds, M. H. Wright, and P. E. Wright, "Convergence properties of the Nelder–Mead simplex method in low dimensions," *SIAM J. Optim.*, vol. 9, pp. 112–147, May 1998.
- [22] D. W. Marquardt, "An algorithm for least-squares estimation of nonlinear parameters," *J. Soc. Ind. Appl. Math.*, vol. 11, no. 2, pp. 431–441, 1963.